

Paramagnetic Impurities in Graphene Oxide

**A. M. Panich, A. I. Shames &
N. A. Sergeev**

Applied Magnetic Resonance

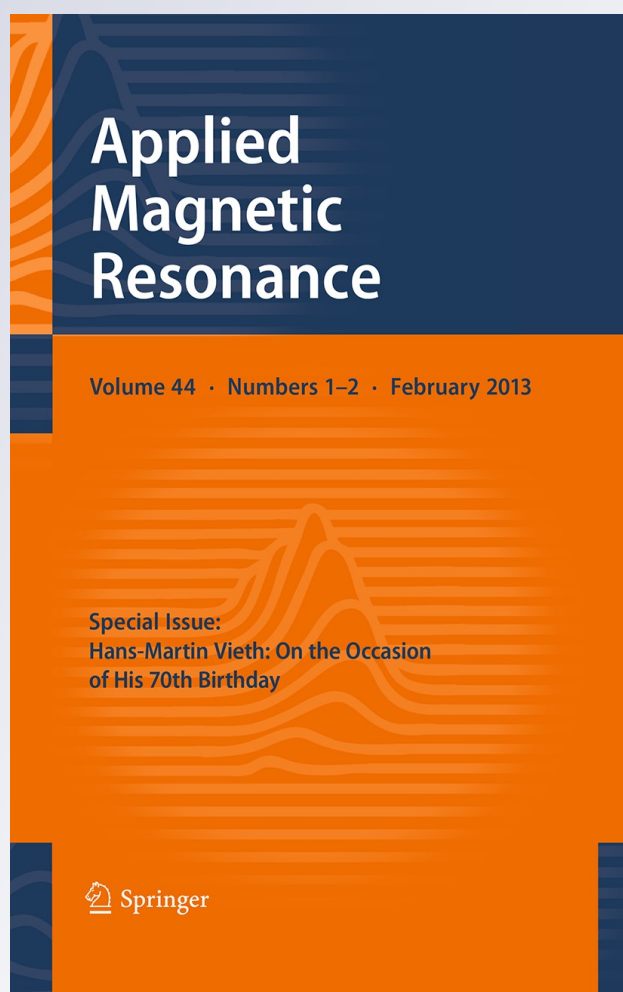
ISSN 0937-9347

Volume 44

Combined 1-2

Appl Magn Reson (2013) 44:107-116

DOI 10.1007/s00723-012-0392-z



Your article is protected by copyright and all rights are held exclusively by Springer-Verlag. This e-offprint is for personal use only and shall not be self-archived in electronic repositories. If you wish to self-archive your work, please use the accepted author's version for posting to your own website or your institution's repository. You may further deposit the accepted author's version on a funder's repository at a funder's request, provided it is not made publicly available until 12 months after publication.

Paramagnetic Impurities in Graphene Oxide

A. M. Panich · A. I. Shames · N. A. Sergeev

Received: 4 July 2012 / Published online: 7 September 2012
© Springer-Verlag 2012

Abstract We report on electron paramagnetic resonance and nuclear magnetic resonance study of graphene oxide produced by the Hummers method. We show that this compound reveals isolated Mn^{2+} ions, which originate from potassium permanganate used in the process of the sample preparation. These ions are likely anchored to the graphene oxide planes and contribute to the ^1H and ^{13}C spin–lattice relaxation.

1 Introduction

One of the crucial bottlenecks for the application of graphene-based systems in materials science is their mass production. Various methods to solve this problem have been suggested; among them, reduction of graphite oxide remains to be the most popular and successful. Unlike graphite, graphite oxide can be dispersed into single-layer *graphene* oxide by sonication or simple stirring in water [1]. The resulting product can be further reduced into graphene or chemically modified graphene-based systems [2]. Herewith, electrical conductivity of the resulting graphene is lower than that of pristine graphene by a factor of 10–100 [3, 4]. Such an effect may be related to different kinds of defects which can affect the electronic, magnetic and other properties of both graphene and graphene oxide. Furthermore, the graphene surface provides a unique opportunity to support chemical impurities that can modify the electronic properties of graphene.

Graphite and graphene oxides are usually prepared by oxidation with $\text{KMnO}_4/\text{H}_2\text{SO}_4$ according to the method of Hummers and Offeman [5]. We have recently

A. M. Panich (✉) · A. I. Shames
Department of Physics, Ben-Gurion University of the Negev,
P.O.Box 653, 84105 Beersheba, Israel
e-mail: pan@bgu.ac.il

N. A. Sergeev
Institute of Physics, University of Szczecin, 70-451 Szczecin, Poland

discovered [6] that graphene synthesized by reduction of graphene oxide reveals Mn^{2+} ions, which originate from potassium permanganate used in the process of the sample preparation. These ions do not exist as a separate phase but form paramagnetic charge-transfer complexes with the graphene planes, which should affect structural, electronic and magnetic properties of graphene important for its applications, e.g., for graphene electronics. One can suggest that similar impurities occur in the precursor graphene oxide. In the present paper, we report on EPR and NMR study of graphene oxide produced by the Hummers method [5] and show that this sample reveals isolated Mn^{2+} ions, which originate from potassium permanganate used in the process of the sample preparation. These ions are likely anchored to the graphene oxide planes and contribute to the ^1H and ^{13}C spin–lattice relaxation.

2 Experimental

The sample under study was prepared in the laboratory of Prof. R. S. Ruoff at the University of Texas at Austin. The parent sample of graphite oxide was synthesized by Hummers method through oxidation of graphite with $\text{KMnO}_4/\text{H}_2\text{SO}_4$ [5]. Then it was dispersed into single-layer graphene oxide by sonication in water [1]. After filtration and drying under 10^{-2} Torr vacuum at room temperature, the graphene oxide was obtained as a powder. We studied this as-prepared sample with its natural composition. As known, (1) this compound reveals some water molecules bound to the surface and entrapped/intercalated between the graphene oxide sheets [2, 7], and (2) its composition changes on heating [8, 9]. To avoid thermal decomposition of the graphene oxide sample [8, 9], no annealing to remove the aforementioned water molecules has been done.

^1H and ^{13}C nuclear magnetic resonance (NMR) spectra and spin–lattice relaxation times were measured in an applied magnetic field $B_0 = 8.0196$ T at resonance frequencies of 341.41 and 85.857 MHz for hydrogen and carbon, respectively, using a Tecmag pulse spectrometer and an Oxford Instruments superconducting magnet. ^{13}C data were collected at room temperature, while ^1H measurements were carried out in the temperature range from 78 to 358 K. Room temperature ($T = 295$ K) electron paramagnetic resonance (EPR) spectra were recorded using a Bruker EMX-220 X-band ($\nu = 9.4$ GHz) spectrometer.

3 Results of the Experiments

Room temperature (RT) EPR spectrum of the powder graphene oxide sample is a superposition of a relatively narrow intensive asymmetric signal (Fig. 1a) and a resolved hyperfine pattern of six broad lines characteristic for isolated Mn^{2+} -containing complexes (Fig. 1b). The shape of asymmetric signal recorded at low incident microwave power level of 200 μW (upper trace in Fig. 1a) resembles polycrystalline pattern for axially distorted $S = 1/2$ system, however, continuous power saturation reveals that this line shape originates from two different carbon-inherited radical-like defects in graphene planes distinguishing by different electron

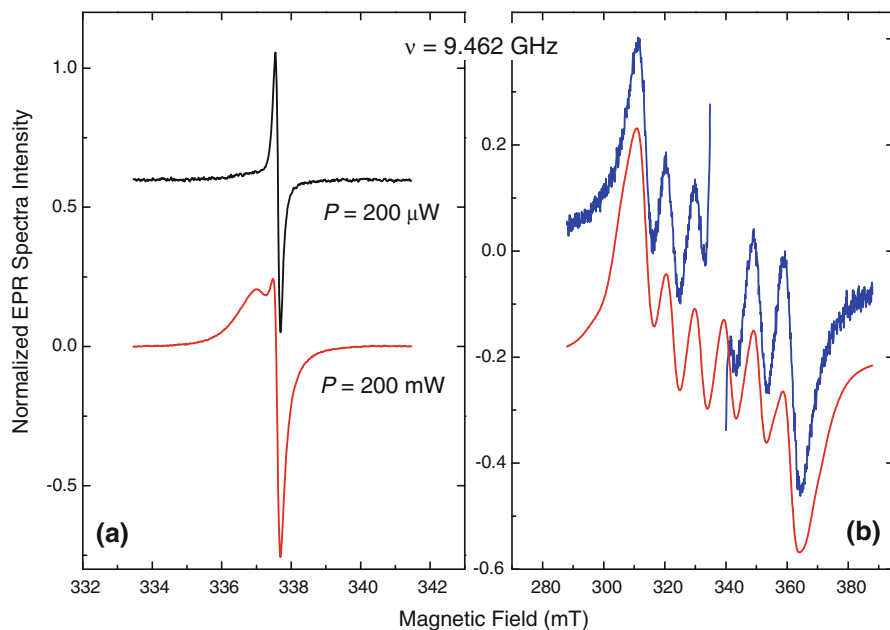


Fig. 1 Room temperature EPR spectra of graphene oxide: **a** zoom of the narrow EPR line recorded at low ($P = 200 \mu\text{W}$) and high ($P = 200 \text{ mW}$) microwave power levels; **b** Blue line shows experimental Mn^{2+} pattern at $P = 20 \text{ mW}$, in which intense narrow EPR signal in the center is cut off. Red line shows the simulation of the powder hyperfine pattern for Mn^{2+} ions with the parameters given in the text (colour figure online)

spin–lattice relaxation rates T_{1e} . At the highest power level (200 mW), the narrower component of this signal becomes saturated, clearly revealing the broader one (lower trace in Fig. 1a). The non-saturated line shape of this signal has been successfully fitted by two Lorentzian components: the narrower component characterized by longer T_{1e} , $g = 2.0030 \pm 0.0002$, $\Delta H_{\text{pp}} = 0.150 \pm 0.005 \text{ mT}$ ($\sim 60\%$ of the total intensity of the radical-like signal) and the broader one with $g = 2.0056 \pm 0.0005$, $\Delta H_{\text{pp}} = 0.56 \pm 0.05 \text{ mT}$ ($\sim 40\%$).

The sextet hyperfine pattern is typical for polycrystalline samples containing magnetically diluted Mn^{2+} complexes ($S = 5/2$, $I = 5/2$) [10]. Simulation (Fig. 1b) reveals that the Mn^{2+} -related polycrystalline EPR pattern may be satisfactorily described by the following spin-Hamiltonian parameters: $g_{\text{iso}} = 2.002$, $A_{\text{iso}} = 9.5 \text{ mT}$, $D \leq 0.004 \text{ cm}^{-1}$ and Lorentzian line width $\delta = 5 \text{ mT}$. The electron spin density was determined to be $1 \times 10^{18} \text{ spin/g}$ for the carbon-inherited paramagnetic defects, while the density of Mn^{2+} ions is $5.5 \times 10^{18} \text{ spin/g}$. The observation of well-resolved hyperfine structure indicates that Mn^{2+} ions exist in the compound as quite magnetically diluted paramagnetic complexes rather than in the form of some impurities of magnetically concentrated Mn salts. These Mn^{2+} ions originate from potassium permanganate used in the process of the sample preparation.

The question is whether Mn^{2+} ions are anchored to the graphene planes, or whether they are present in the compound as a separate phase. The answer may be

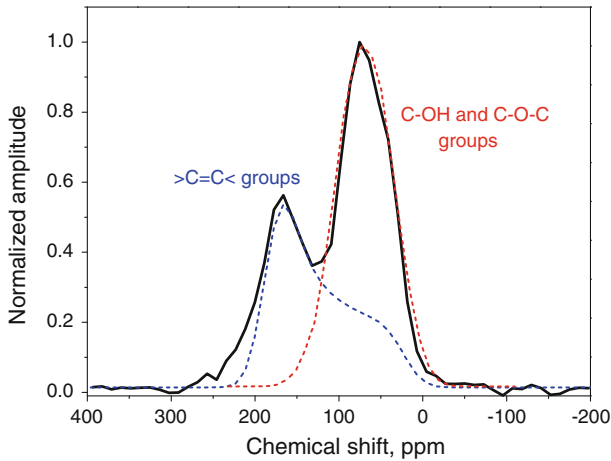


Fig. 2 Static room temperature ^{13}C NMR spectrum of graphene oxide (colour figure online)

received from the measurements of the ^{13}C spin–lattice relaxation time and its comparison with that found for graphene [6]. The point is that if paramagnetic ions are anchored to the graphene, they would reduce the nuclear spin–lattice relaxation time T_1 due to interaction of ^{13}C nuclear spins with uncoupled electron spins. While in the case that paramagnetic inclusions are present in the material as a separate phase, the above effect is negligible, since T_1 is proportional to the sixth power of the distance between spins.

Let us now discuss our NMR measurements. Static room temperature ^{13}C NMR spectrum of graphene oxide is shown in Fig. 2. It is deconvoluted into two components. The first asymmetric line with chemical shift $\sigma \approx 130$ ppm and chemical shift anisotropy $\Delta\sigma \approx 150$ ppm is characteristic of aromatic carbons and thus is assigned to sp^2 carbon atoms of the graphene sheet. The second component is assigned to overlapping lines resulting from C–OH and C–O–C groups with $\sigma = 57$ and 68 ppm. These data are in agreement with previously measured ^{13}C spectra of graphene oxide [2, 7, 11, 12].

Room temperature measurement of the spin–lattice relaxation time in graphene oxide shows that $T_1(^{13}\text{C}) = 36.9 \pm 3.5$ s. Herewith, the magnetization recovery is well described by a stretched exponent $M(t) = M_\infty \left\{ 1 - \exp \left[- \left(\frac{t}{T_1} \right)^\alpha \right] \right\}$, where M_∞ is the equilibrium magnetization and $\alpha \approx 0.8$. The obtained T_1 is several times shorter than that in graphite and polyhedral multilayer carbon onions, which show $T_1(^{13}\text{C}) = 110$ and 152 s, respectively [13, 14] (Table 1), despite the radical-like paramagnetic center densities of 2.8×10^{17} spins g^{-1} for graphite and 5×10^{17} spins g^{-1} for localized spins in carbon onions are of the same order of magnitude as in graphene oxide under study (Table 1). (Herewith, the carbon onions also show 7×10^{18} spins g^{-1} for the quasi-localized electron spins). Therefore, one can suggest that the observed reduction of T_1 is caused by the interaction of ^{13}C spins with uncoupled electron spins of paramagnetic Mn^{2+} ions, which opens an additional channel for the nuclear spin–lattice relaxation [15–20]. Thus, the Mn^{2+}

Table 1 Density of paramagnetic centers and ^{13}C spin–lattice relaxation time T_1 in graphene, graphene oxide, graphite and carbon onions

Compound	N_S (spin/g)	$N(\text{Mn}^{2+})$ (spin/g)	T_1 (s)
Graphene [6]	7×10^{17}	10^{20}	1.9
Graphene oxide (this work)	1×10^{18}	5.5×10^{18}	36.9
Graphite [13, 14]	2.8×10^{17}	–	110
Polyhedral multi-shell carbon onions [13, 14]	5×10^{17} to 7×10^{18}	–	152

Here N_S and $N(\text{Mn}^{2+})$ are the densities of the radical-like carbon-inherited defects and Mn^{2+} ions, respectively

ions are likely anchored to the graphene planes or probably to the hydrogen atoms of the C–OH groups.

Let us discuss this opportunity by comparing the obtained T_1 data of graphene oxide with those of graphene prepared by Hummer's method [6] (Table 1). Graphene shows much shorter spin–lattice relaxation time ($T_1(^{13}\text{C}) = 1.9$ s) than that of graphene oxide. However, for graphene we found 7×10^{17} and 10^{20} spin/g for the carbon-inherited defects and Mn^{2+} -complexes, respectively [6]. Thus, the density of the radical-like paramagnetic defects is of the same order of magnitude in both graphene oxide under study and graphene sample, while the amount of the Mn^{2+} ions in graphene oxide under study is almost 20 times smaller than that in graphene (Table 1). The value of $N(\text{Mn}^{2+}, \text{graphene})/N(\text{Mn}^{2+}, \text{graphene oxide}) = 18.2$ is very close to the inverse ratio of the corresponding relaxation times $T_1(\text{graphene oxide})/T_1(\text{graphene}) = 36.9/1.9 = 19.4$. Since for diluted paramagnetic systems the nuclear spin–lattice relaxation time is inversely proportional to the density of paramagnetic centers, this result corresponds well to the model in which the Mn^{2+} ions are bound to the graphene sheets and form charge-transfer complexes with graphene oxide similar to graphene sample studied in Ref. [6].

Let us now move to the ^1H NMR experiments. The main sources of hydrogen in graphene oxide are (1) hydroxyl (C–OH) groups and (2) water molecules bound to the surface and those entrapped/intercalated between the graphene oxide layers [2, 7]. Occurrence of the hydrogen atoms in the graphene oxide sample under study is well seen in the ^1H NMR measurements. Static RT ^1H NMR spectrum of graphene oxide (Fig. 3) is a narrow line with line width $\Delta\nu = 4.2$ kHz. This line is significantly broadened on cooling, which is typical for progressive freezing of water mobility. One can find from Fig. 3 that the spectrum at $T = 90$ K shows some poorly expressed fine structure, which is better seen in the first derivative of the spectrum. This spectrum can be interpreted as consisting of two lines. Here narrower component is attributed to the C–OH groups, while the broad component is assigned to the frozen water molecules showing well known Pake doublet [21], arising from the strong dipole–dipole coupling among two ^1H spins in the H_2O molecule.

The noticeable line width of the narrower component at $T = 90$ K is caused by dipole–dipole interaction of protons of C–OH group and water molecule, evidencing that protons of adsorbed/intercalated water molecules are positioned close to the

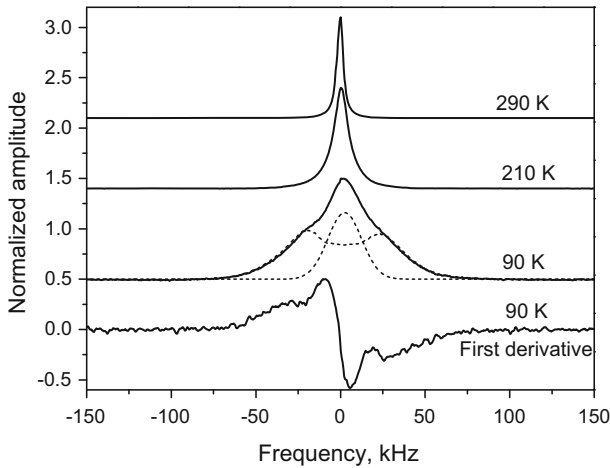


Fig. 3 ^1H NMR spectra of graphene oxide at different temperatures. Deconvolution of the spectrum measured at $T = 90\text{ K}$ into two components is shown by *dashed lines*. First derivative of this spectrum is given at the *bottom of the figure*

C–OH groups, as suggested by He et al. [7]. The line broadening on cooling is well reflected in the significant increase of the second moment of the resonance line shown in Fig. 4.

The above conclusions are well supported by ^1H spin–lattice relaxation measurements (Fig. 5). Temperature dependence of the ^1H spin–lattice relaxation rate exhibits a characteristic curve with a maximum of R_1 (and a minimum of T_1) at $\sim 330\text{ K}$ that appears due to fluctuations of dipole–dipole interactions of hydrogen spins caused by fast molecular motion [22]. For this relaxation mechanism, the Bloembergen–Purcell–Pound (BPP) theory [22] yields an expression for the relaxation rate $R_{1n} = 1/T_{1n}$ as

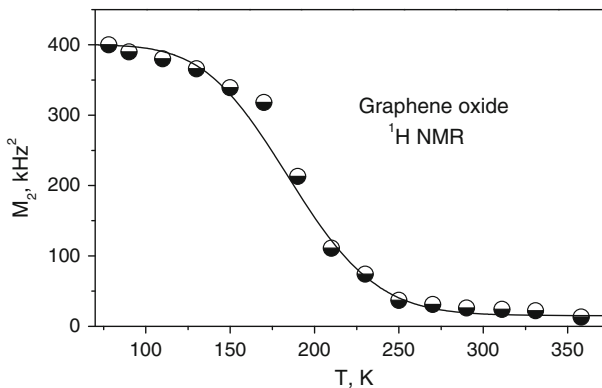


Fig. 4 Temperature dependence of the second moment M_2 of the ^1H spectra in graphene oxide

$$R_{1n} \equiv T_{1n}^{-1} = \frac{2}{3} \Delta M_2 \left[\frac{\tau_c}{1 + \omega_0^2 \tau_c^2} + \frac{4\tau_c}{1 + 4\omega_0^2 \tau_c^2} \right], \tag{1}$$

where $\omega_0 = \gamma B_0$ is the nuclear Larmor frequency, τ_c is the correlation time of the molecular rotation, $\Delta M_2 = M_2 - \langle M_2 \rangle$ is the reduction of the second moment caused by the motion of the water molecules, M_2 is the second moment of the rigid lattice, and $\langle M_2 \rangle$ is the second moment of the NMR spectrum averaged by molecular motion [22]. From Eq. (1) we can find that $R_1 \sim \tau_c$ for $\omega_0 \tau_c \ll 1$, while $R_1 \sim 1/\tau_c$ for $\omega_0 \tau_c \gg 1$, with a maximum of R_1 (and minimum of T_1) in the intermediate region at $\omega \tau_c = \frac{1}{\sqrt{2}}$. Since the correlation time τ_c caused by the molecular motion usually follows the Arrhenius-type temperature dependence $\tau_c = \tau_0 \exp(E_a/k_B T)$ [23], the asymptotic behavior of $\log R_1(\frac{1}{T})$ is represented by straight lines. Just such a behavior is obtained in our experiment in the temperature range from 270 to 170 K. This mechanism results here in a deceleration of the relaxation rate and increase in relaxation time on cooling. The deviation from the linear slowdown below $T \sim 170$ K and gradual reaching a plateau is known to be caused by interaction of nuclear spins with paramagnetic ions [15, 20, 24], whose contribution to the nuclear spin–lattice relaxation rate is

$$R_{1ne} \equiv T_{1ne}^{-1} = \gamma_H^2 \langle H_L^2 \rangle \cdot \frac{\tau_{ce}}{1 + (\omega_0 \tau_{ce})^2}, \tag{2}$$

where the squared averaged local field on nuclei produced by unpaired electron spins is

$$\langle H_L^2 \rangle = \frac{2}{5} \mu_p^2 \frac{N_e}{N_n} \sum_i R_{ij}^{-6}. \tag{3}$$

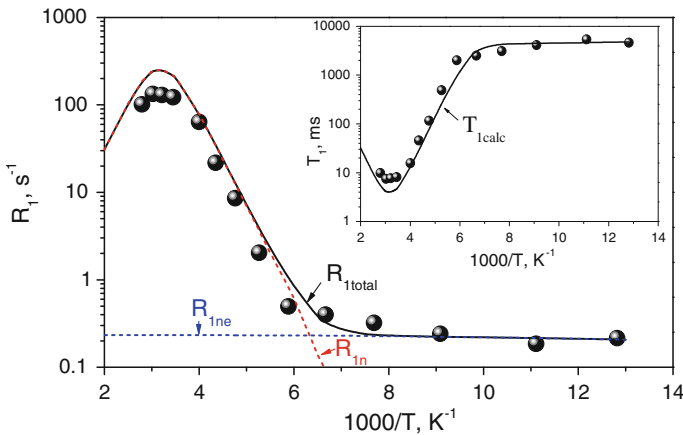


Fig. 5 Dependence of ^1H spin–lattice relaxation rate R_1 in graphene oxide in semi-logarithmic scale on reciprocal temperature. *Filled circles* experiment, *red dashed line* contribution of motion of hydrogen atoms, *blue dashed line* contribution of paramagnetic centers, *black solid line* total calculated R_1 . Temperature dependence of ^1H spin–lattice relaxation time $T_1 = 1/R_{1\text{total}}$ is shown in *inset* (colour figure online)

Here $\mu_p^2 = J(J + 1)\gamma_j^2\hbar^2$ is the squared magnetic moment of the paramagnetic center, N_e is the density of paramagnetic centers, N_n is the density of the hydrogen spins, R_{ij} is the distance between the electron and nuclear spins, and τ_e is the electron correlation time. The latter follows an Arrhenius-type temperature dependence $\tau_e = \tau_{0e} \exp(E_{ac}/k_B T)$ and varies in the range of 10^{-9} to 10^{-12} s, thus usually $\omega_0\tau_e \ll 1$ and $R_1 \sim \tau_e$, and the magnetic contribution to the nuclear spin–lattice relaxation rate increases on cooling, which results in fast and weakly (owing to small E_{ac}) temperature-dependent relaxation at low temperatures [15, 24–26]. This relaxation mechanism dominates at low temperatures while the motional contribution is not effective. The total relaxation rate is

$$R_1 = R_{1n} + R_{1ne}, \tag{4}$$

and the interplay of paramagnetic and motional contributions yields a characteristic $R_1(T)$ dependence observed in our experiment. Therefore, our ^1H measurements support the above conclusion that Mn^{2+} ions are attached to the graphene oxide planes, herewith being positioned close to the hydrogen atoms. The calculated parameters of expressions Eqs. 1–3, which fit the experimental data, are given in Table 2. Since graphene oxide is built of aromatic islands of variable size, which are separated from each other by aliphatic 6-membered rings containing C–OH and epoxy groups and double bonds, and since the distribution of functional groups in every oxidized aromatic ring is not identical and both the oxidized rings and aromatic entities are distributed randomly [7], we suggested in our calculations that proton mobility in graphene oxide is inhomogeneous and is characterized by a normal distribution of the activation energies

$$p(E_a) = \frac{1}{\sqrt{2\pi}\sigma_E} \exp\left\{-\frac{E_a - \bar{E}_a}{2\sigma_E^2}\right\}. \tag{5}$$

The calculated parameter σ_E is given in Table 2.

4 Discussion

Recent calculations predict several models of manganese ion anchoring to graphene and graphane. Wu et al. [27] reported on the first-principle’s calculation of graphene doped with the Mn atom by substituting a carbon atom in the lattice, which can also be regarded as a Mn atom being adsorbed on a vacancy site in the graphene sheet.

Table 2 Calculated parameters of Eqs. 1–3 and 5 that describe proton mobility and relaxation via paramagnetic centers

ΔM_2 (kHz ²)	τ_0 (s)	\bar{E}_a (kcal/mol)	σ_E (kcal/mol)	τ_{0e} (s)	E_{ac} (kcal/mol)	$\gamma_H^2 \langle H_L^2 \rangle$ (rad \times kHz) ²
385	10^{-13}	5.00	0.2	4×10^{-10}	0.1	1,000

Here $\gamma_H = 26.74$ rad \times kHz/G

Herewith the Mn atom strongly binds with three neighbor carbon atoms, forming a charge-transfer complex with covalent Mn–C bonds.

AlZahrani [28] discussed four structural models for the Mn-adsorbed graphene with Mn atom (1) resides the hollow site, (2) on the top of the middle C–C dimer, (3) on the top of the C atom, and (4) substitutes one of the C atoms. Among these structures, it was found that the Mn atom is not likely to substitute the C atom. Alternatively, the Mn atom prefers to be interstitially adsorbed at the center of the hexagon (hollow site), forming covalent bonds with the nearest carbon atoms. Unlike the results on Mn-doped graphane [29] showing that transition metal atom fills/occupies the vacancy made by a missing hydrogen atom, AlZahrani [28] showed that the Mn adatom in graphane prefers to adsorb on the top of a carbon atom, forming a bridge with the uppermost hydrogen atoms.

All these three models actually predict occurrence of charge-transfer complexes between Mn ions and graphene or graphane. Such a prediction can be extended for the graphene oxide as well, correlating with our experimental data, which shows that the impurity Mn^{2+} ions are attached to the graphene oxide layers rather than form a separate phase.

In order to support this hypothesis, an attempt was made to extract an average value for the Mn–C and Mn–H distances. Using Eqs. 2 and 3, we calculated $R(\text{Mn–C}) = 4.5 \text{ \AA}$ and $R(\text{Mn–H}) = 4.7 \text{ \AA}$, much longer than the sum of covalent radii of Mn and C, 2.27 \AA , and Mn and H, 1.87 \AA [28]. However, we note that since the density of paramagnetic ions is several orders of magnitude smaller than the densities of H and C atoms, the real distances between them vary in a wide range, from those corresponding to the covalent bond to much longer spacings to the distant host atoms [30]. Therefore, the calculated average separations between the Mn^{2+} ions and host atoms appeared to be rather long.

In addition, we note that since water mobility at high temperature averages out all dipole–dipole interactions between diffusing H_2O molecules and OH groups, the corresponding value of the second moment at 358 K reflects the dipole–dipole coupling among the protons of fixed hydroxyl groups. For two neighboring OH groups, the value of $M_2 = 13 \text{ kHz}^2$ at $T = 358 \text{ K}$ yields separation between two hydrogen atoms as 2.82 \AA . This is in good agreement with the structural model of graphene oxide [2, 7, 11], in which two hydroxyl groups neighbor each other. We note, however, that owing to inhomogeneity of the positioning of these groups, the distance between the hydrogen atoms is likely variable.

5 Summary

Summarizing, our EPR and NMR measurements demonstrate that graphene oxide prepared by the Hummers method reveals isolated Mn^{2+} ions, which likely form paramagnetic charge-transfer complexes with the graphene planes and contribute to the ^1H and ^{13}C spin–lattice relaxation.

Acknowledgments We thank J. Edgeworth and R. S. Ruoff for supplying us with the graphene oxide sample.

References

1. S. Stankovich, D.A. Dikin, G.H.B. Dommett, K.M. Kohlhaas, E.J. Zimney, E.A. Stach, R.D. Piner, S.T. Nguyen, R.S. Ruoff, *Nature* **442**, 282 (2006)
2. S. Stankovich, D.A. Dikin, R.D. Piner, K.A. Kohlhaas, A. Kleinhammes, Y. Jia, Y. Wu, S.T. Nguyen, R.S. Ruoff, *Carbon* **45**, 1558 (2007)
3. V. Lopez, R.S. Sundaram, C. Gomez-Navarro, D. Olea, M. Burghard, J. Gomez-Herrero, F. Zamora, K. Kern, *Adv. Mater.* **21**, 4683 (2009)
4. V.C. Tung, M.J. Allen, Y. Yang, R.B. Kaner, *Nat. Nanotechnol.* **4**, 25 (2009)
5. W.S. Hummers, R.E. Offeman, *J. Am. Chem. Soc.* **80**, 1339 (1958)
6. A.M. Panich, A.I. Shames, A.E. Aleksenskii, A. Dideikin, *Solid State Commun.* **152**, 466 (2012)
7. H. He, Th Riedl, A. Lerf, J. Klinowski, *J. Phys. Chem.* **100**, 19954 (1996)
8. Daniel R. Dreyer, Sungjin Park, Christopher W. Bielawski, Rodney S. Ruoff, *Chem. Soc. Rev.* **39**, 228–240 (2010)
9. W. Gao, L.B. Alemany, L. Ci, P.M. Ajayan, *Nature Chem.* **1**, 403 (2009)
10. A. Abragam, B. Bleaney, *Electron Paramagnetic Resonance of Transition Ions* (Oxford University Press, Oxford, 1970)
11. A. Lerf, H. He, M. Forster, J. Klinowski, *J. Phys. Chem. B* **102**, 4477 (1998)
12. L.B. Casabianca, M.A. Shaibat, W.W. Cai, S. Park, R. Piner, R.S. Ruoff, Y. Ishii, *J. Am. Chem. Soc.* **132**, 5672 (2010)
13. A.I. Shames, E.A. Katz, A.M. Panich, D. Mogilyansky, E. Mogilko, J. Grinblat, V.P. Belousov, I.M. Belousova, A.N. Ponomarev, *Diam. Relat. Mater.* **18**, 505 (2009)
14. A.I. Shames, E.A. Katz, A.M. Panich, D. Mogilyansky, E. Mogilko, J. Grinblat, V.P. Belousov, I.M. Belousova, A.N. Ponomarev, *Closed π -electron Network in Large Polyhedral Multi-shell Carbon Nanoparticles* (Los Alamos National Laboratory, Los Alamos). Preprint Archive, Condensed Matter, April 20, 2009, <http://arxiv.org/abs/0904.2647>
15. A.M. Panich, N.A. Sergeev, *Phys. B* **405**, 2034 (2010)
16. A.M. Panich, A.I. Shames, H.-M. Vieth, E. Ōsawa, M. Takahashi, A. Ya, Vul'. *Eur. Phys. J. B* **52**, 397 (2006)
17. A.M. Panich, A.I. Shames, O. Medvedev, V.Yu. Osipov, A.E. Alexenskii, A.Ya. Vul', *Appl. Magn. Reson.* **36**, 317 (2009)
18. A.M. Panich, H.-M. Vieth, A.I. Shames, N. Froumin, E. Ōsawa, A. Yao, *J. Phys. Chem. C* **114**, 774 (2010)
19. A.M. Panich, A. Altman, A.I. Shames, VYu. Osipov, A.E. Alexenskiy, A. Ya, Vul'. *J. Phys. D Appl. Phys.* **44**, 125303 (2011)
20. A.M. Panich, G.B. Furman, *Diam. Relat. Mater.* **23**, 157 (2012)
21. G.E. Pake, *J. Chem. Phys.* **16**, 327 (1948)
22. N. Bloembergen, E.M. Purcell, R.V. Pound, *Phys. Rev.* **73**, 679 (1948)
23. A. Abragam, *The Principles of Nuclear Magnetism* (Clarendon Press, Oxford, 1961)
24. E. Fukushima, S.B.W. Roeder, *Experimental Pulse NMR: A Nuts and Bolts Approach* (Addison-Wesley, London, 1981)
25. A.M. Panich, C.L. Teske, W. Bensch, *Phys. Rev. B* **73**, 115209 (2006)
26. A.M. Panich, A.I. Shames, H. Selig, *J. Phys. Chem. Solids* **63**, 483 (2002)
27. M. Wu, C. Cao, J.Z. Jiang, *New J. Physics* **12**, 063020 (2010)
28. A.Z. AlZahrani, *Phys. B* **407**, 992 (2012)
29. C.-K. Yang, *Carbon* **48**, 3901 (2010)
30. W.E. Blumberg, *Phys. Rev.* **119**, 79 (1960)